

THE PROPERTIES OF HEAVY ELEMENTS IN GIANT PLANET ENVELOPES

FRANÇOIS SOUBIRAN¹ AND BURKHARD MILITZER^{1,2}

¹Department of Earth and Planetary Science, University of California, Berkeley, CA 94720, United States
and

²Department of Astronomy, University of California, Berkeley, CA 94720, United States

ABSTRACT

The core accretion model for giant planet formation suggests a two layer picture for the initial structure of Jovian planets, with heavy elements in a dense core and a thick H-He envelope. Late planetesimal accretion and core erosion could potentially enrich the H-He envelope in heavy elements, which is supported by the three-fold solar metallicity that was measured in Jupiter’s atmosphere by the Galileo entry probe. In order to reproduce the observed gravitational moments of Jupiter and Saturn, models for their interiors include heavy elements, Z , in various proportions. However, their effect on the equation of state of the hydrogen-helium mixtures has not been investigated beyond the ideal mixing approximation. In this article, we report results from *ab initio* simulations of fully interacting H-He- Z mixtures in order to characterize their equation of state and to analyze possible consequences for the interior structure and evolution of giant planets. Considering C, N, O, Si, Fe, MgO and SiO₂, we show that the behavior of heavy elements in H-He mixtures may still be represented by an ideal mixture if the effective volumes and internal energies are chosen appropriately. In the case of oxygen, we also compute the effect on the entropy. We find the resulting changes in the temperature-pressure profile to be small. A homogeneous distribution of 2% oxygen by mass changes the temperature in Jupiter’s interior by only 80 K.

Keywords: Physical Data and Processes: equation of state; planets and satellites: gaseous planets; planets and satellites: Jupiter, Saturn, Uranus, Neptune.

1. INTRODUCTION

Despite numerous observations of giant planets in our solar system (Bolton 2010; Jones *et al.* 2015) and the extrasolar campaigns (Wright *et al.* 2011; Schneider *et al.* 2011), our understanding of the structure, evolution, and formation of Jovian planets remains uncertain (Guillot & Gautier 2015). Largely, the uncertainty is due to the fact that the observations of Jovian planets only provide data on global properties, which limits the constraints that can be placed on interior properties. While future observations, such as the Juno mission, will provide more detailed data, additional constraints on Jovian interiors can also be gleaned from advances in numerical simulations (Militzer 2013) and experiments (Brygoo *et al.* 2015) on high density matter and the subsequent improvements in planetary models (Nettelmann *et al.* 2012; Helled & Guillot 2013; Hubbard & Militzer 2016).

Even in the solar system, the exact composition of the gaseous giant planets is still not very well constrained because the composition of the observable atmosphere is not necessarily representative of the entire planet.

Following the core-accretion hypothesis (Pollack *et al.* 1996), Jupiter and Saturn were formed by a rapid accretion of solid material until a critical mass of approximately $10 M_{\oplus}$ had been reached, which triggers a substantial gas accretion. Once the envelope is as massive as the core, it even becomes a run-away accretion that stops when all the gas in the nebula has disappeared, after about 10 Myr. This minimum mass of $10 M_{\oplus}$ provides also a lower bound for the average metallicity of Jupiter and Saturn. As the total mass of Jupiter (resp. Saturn) is $317.8 M_{\oplus}$ (resp. $95.1 M_{\oplus}$) (Baraffe *et al.* 2010), the minimal metallicity is $Z_J = 0.031$ (resp. $Z_S = 0.105$) which is higher than the solar value of $Z_{\odot} = 0.0149$ (Lodders 2003). But this is only a minimum value, and for Jupiter, the Galileo entry probe measured an atmospheric metallicity of 3 times the solar value (Wong *et al.* 2004) for instance.

The dichotomy between a dense core and a H-He envelope is however, at best, only an approximated view of the giant planets as there are at least five different reasons why the heavy element distribution in giant planets is uncertain. The first one comes from the forma-

tion of the planet. During the gas accretion, the planet kept accreting additional planetesimals and it is unclear whether they dissolved in the envelope or reached the core (Fortney *et al.* 2013).

The second reason is the possible erosion of the core as proposed by Stevenson (1982), which could trigger a redistribution of the heavy elements of the core throughout the envelope. This possibility has been recently investigated with *ab initio* simulations, which predicted that all the dominant species in the core are miscible in metallic hydrogen (Wilson & Militzer 2012a,b; Wahl *et al.* 2013; González-Cataldo *et al.* 2014).

However, and this is the third reason, the kinetics of the erosion process is very poorly constrained and could be very slow. Once dissolved in hydrogen, the heavy elements may not be efficiently redistributed throughout the envelope because the density contrast may be too high for the convection to advect these elements against the gravitational forces. Thus, a semi-convective pattern is likely to set in, inducing a gradient of composition in the layers close to the core (Leconte & Chabrier 2012, 2013).

An other origin of heterogeneity in giant planet envelopes could come from the phase separation of H-He which has been proposed as an explanation of the excess of luminosity of Saturn (Stevenson & Salpeter 1977; Fortney & Hubbard 2004). The exact phase diagram is still controversial despite recent work using *ab initio* simulations (Lorenzen *et al.* 2009, 2011) and even thermodynamic integrations to properly account for the non-ideal entropy (Morales *et al.* 2009, 2013). However, some experimental constraints should be available shortly using reflectivity measurements in laser-driven shock experiments (Soubiran *et al.* 2013). But if the phase separation occurs in a giant planet, it could also inhibit the advection of heavy elements from the deep interior to the external layers as the convection would most likely be rendered less efficient by the phase separation.

The last reason of uncertainty comes from the possible partitioning of the heavy elements due to the miscibility difference with helium and with hydrogen. It has been suggested, for instance, as an explanation for the strong depletion in neon in the atmosphere of Jupiter (Wilson & Militzer 2010).

We therefore need to have better constraints on the distribution of the heavy elements. They may come from both observations and more detailed models. Measurements of the gravitational field of Jupiter and Saturn via the study of the trajectory of their satellites but also via direct measurements from spacecrafts such as Cassini and Juno can give strong constraints on the gravitational moments of the planet and thus on the mass distribution. A new field is also emerging: seismology of

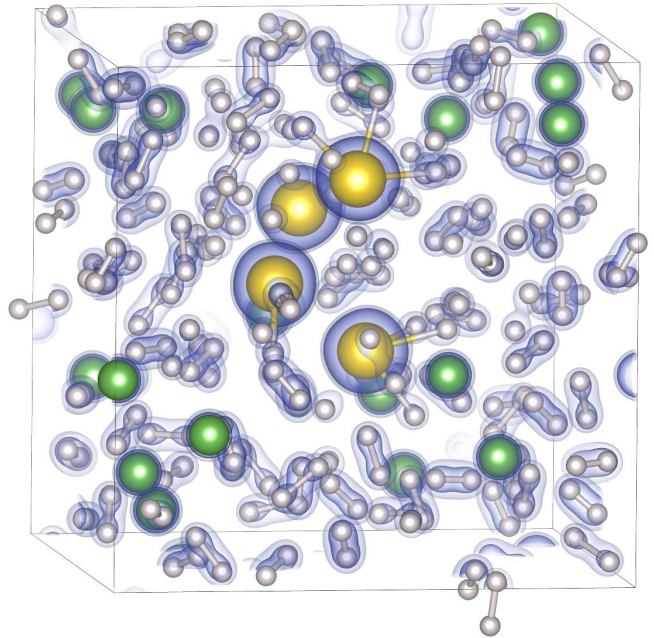


Figure 1. Snapshot of a simulation box containing 220 H (white), 18 He (green) and 4 Fe (yellow) atoms at 2000 K and 60 GPa. We used a distance analysis to identify the chemical bonds. The isosurfaces represent the electronic density.

giant planets. Recent results using planetary oscillations (Gaulme *et al.* 2011) and more importantly through ring seismology (Fuller *et al.* 2014a; Fuller 2014b) have started to demonstrate its potential and will most likely lead to additional constraints.

Theorists can also help to constrain the possible structures by building detailed models including accurate physical properties of matter at high density. Improvements in *ab initio* simulations over the past two decades offered the possibility to compute precise equations of state (EOS). Recently an updated EOS of H-He has been developed by Militzer (2013). Concerning the heavy elements, different EOSs have been used in giant planet models (see Baraffe *et al.* (2008) for a review of the common EOSs). Recent models showed that the heavy elements altered the density profile and therefore the structure of the planet (Hubbard & Militzer 2016), as well as its evolution (Baraffe *et al.* 2008). However, these models rely on the assumption that the multi-component mixtures of interest are ideal mixtures with an isothermal-isobaric additive mixing rule. Under this assumption, one derives all extensive thermodynamic properties of a mixture – volume, internal energy,... – by adding up the contributions from the individual pure species at a given temperature and pressure. Such a mixing rule neglects all the inter-species interactions, although they may be much more important than the intra-species ones. For instance, in the diluted limit, a heavy atom only interacts with the H-He – solvent – atoms while, in the ideal mixing approximation, the

properties of the heavy species are taken from a system of heavy atoms only.

Once the Juno mission will have measured the gravitational moments of Jupiter with high precision, interior models with various amounts of heavy elements in the envelope and different core sizes will be constructed to match these measurements. This will improve our understanding of the interior structure and the evolution of Jupiter. One goal of this paper is to make this analysis more accurate by going beyond the standard ideal mixing rule and by properly characterizing the influence of heavy elements on a H-He envelope.

In this article, we investigate the thermodynamic properties of ternary mixtures of hydrogen, helium and heavy elements – namely carbon, nitrogen, oxygen, silicon, iron as well as magnesium oxide and silicon dioxide – under conditions relevant for the giant planet interiors. We used *ab initio* simulations to determine the influence of these seven elements on the density and the internal energy. On the case of oxygen, we also studied the influence on the entropy, which is essential to determine the pressure-temperature profile in giant planet envelopes.

From our analysis we determined that the ternary mixtures can indeed be very well described by an ideal isothermal-isobaric mixing of H-He on one side and the heavy element on the other, provided however that effective volume or energy of the heavy species are chosen appropriately. Both properties may differ from the properties from those of the pure species at the same temperature and conditions. They may furthermore be affected by the dissociation of hydrogen.

We also performed entropy calculations for H-He-O ternary mixtures. We show that the addition of heavy element, homogeneously throughout the envelope of a giant planet, has only a marginal influence on the pressure-temperature and on the density profiles. Last, we explore the influence of the heavy elements on the mass-radius relationship of giant planets.

2. SIMULATION METHODS

We performed molecular dynamics (MD) simulations with forces derived from density functional theory (DFT) (Hohenberg & Kohn 1964) to treat the quantum behavior of the electrons. We performed the simulations with the Vienna *ab initio* simulation package (Kresse & Furthmüller 1996). We used cubic cells with periodic boundary conditions. Starting from cells with 220 hydrogen and 18 helium atoms (Militzer 2013), we added from 2 to 8 atoms or molecules of heavy elements – we considered C, N, O, Si, Fe, MgO and SiO₂. As an example, Fig. 1 shows a representative snapshot of a simulation of H, He and Fe.

We performed the dynamics with a 0.2 fs time step, for a trajectory of at least 1 ps. The temperature

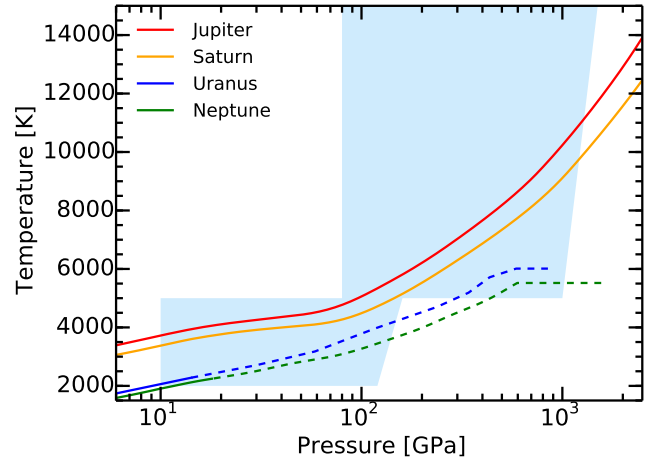


Figure 2. Pressure vs temperature profiles of the solar giant planets. Jupiter and Saturn adiabatic profiles are from Militzer & Hubbard (2013) and Uranus and Neptune models are from Nettelmann *et al.* (2013). The dashed lines indicate the part of the planets that is expected to be mostly made of heavy elements. The shaded region represents the range of parameters we explored.

was controlled by a Nosé thermostat (Nosé 1984, 1991). We solved the DFT part using the Kohn-Sham scheme (Kohn & Sham 1965) at finite temperature (Mermin 1965) with a Fermi-Dirac distribution function. We employed Perdew, Burke and Ernzerhof (PBE) (Perdew *et al.* 1996) exchange-correlation functionals. This functional provided accurate results for numerous systems including the pure species presently considered (Caillet *et al.* 2011; Militzer 2009; Benedict *et al.* 2014; Driver *et al.* 2015; Driver & Militzer 2016; Militzer & Driver 2015; Denœud *et al.* 2014). We employed standard VASP projector augmented wave (PAW) pseudopotentials (Blöchl 1994). The cutoff radius was 0.8 a_0 for hydrogen, 1.1 a_0 for helium, 1.1 a_0 for carbon, nitrogen and oxygen, each with a 1s² frozen core, 2.0 a_0 for magnesium with a 1s²2s² core, 1.9 a_0 for silicon with a 1s²2s²2p⁶ core, and 2.2 a_0 for iron with a 1s²2s²2p⁶3s²3p⁶ core, where a_0 stands for the Bohr radius. We used the frozen core approximation to speed-up the calculations and because we are at low enough density for the core energy level shift towards the continuum to be negligible, as well as at low enough temperatures for the thermal ionization of the core levels to be insignificant (Driver *et al.* 2015). The energy cutoff for the plane-wave basis was set to 1200 eV. The number of electronic bands was adapted to the species, the density and the temperature conditions in order to completely cover the spectrum of the fully and partially occupied eigenstates. We sampled the Brillouin zone with the Baldereschi point (Baldereschi 1973). Militzer (2013) showed that the convergence of the calculation for H-He was very good with this choice of parameters.

On a subset of simulations, we also performed ther-

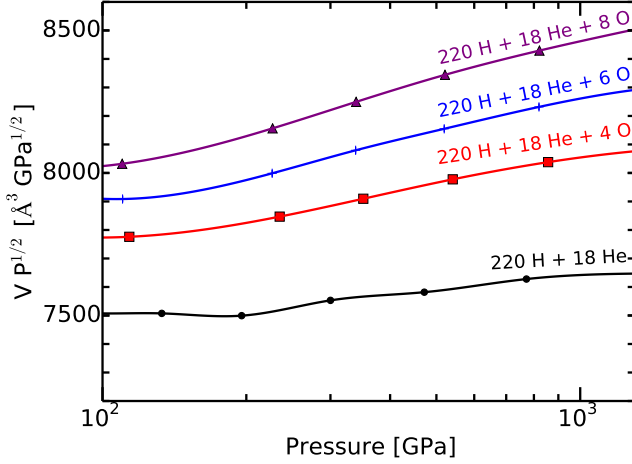


Figure 3. Volume of the H-He-O simulation cell multiplied by the square root of the pressure – to magnify the differences – as a function of the pressure at 10000 K for different oxygen composition. The symbols show the numerical results and the curves represent spline interpolations.

modynamic integrations to obtain the Helmholtz free energy and the entropy. We progressively switched the interactions in the system from the potential given by the DFT U_{DFT} to a classical potential U_{cl} . This methods has been applied on many systems (de Wijs *et al.* 1998; Morales *et al.* 2009; Wilson & Militzer 2010, 2012a,b; McMahon *et al.* 2012; Wahl *et al.* 2013, 2015). It provides the Helmotz free energy difference between the two systems:

$$F_{\text{DFT}} - F_{\text{cl}} = \int_0^1 d\lambda \langle U_{\text{DFT}} - U_{\text{cl}} \rangle_{\lambda}, \quad (1)$$

where the parameter λ defines the hybrid potential $U_{\lambda} = U_{\text{cl}} + \lambda(U_{\text{DFT}} - U_{\text{cl}})$ and the average refers to an average over configurations computed with the potential U_{λ} . For the classical potential, we used a set of non-bonding pair potentials fitted on the DFT forces. More details of the integration are given in Soubiran & Militzer (2015a) and in Wahl *et al.* (2015).

In order to determine the different thermodynamic quantities as a function of the pressure rather than the density, we used a spline interpolation method. For the pressure and the volume, we used the logarithmic values as variables for the interpolation. Fig. 3 shows an example of an interpolation.

3. RESULTS

We investigated the properties of ternary mixtures with H-He and seven different heavy elements: C, N, O, Si, Fe, MgO, SiO₂. We explored the thermodynamic properties on two different domains: from 10 to 150 GPa and 2000 to 5000 K, and from 80 to 1500 GPa and 5000 to 15000 K – see Fig. 2. The thermodynamic data are presented in Tabs. 3 and 4. We also added the

numerical values of the effective properties we computed in Tab. 5. For each simulation we computed a one- σ errorbar for the thermodynamic data, based on a block averaging method (Rapaport 2004). We used standard error propagation methods for the effective properties.

3.1. Effective volume

For each heavy element, we performed MD-DFT simulations for 3 different concentrations, keeping the number of hydrogen and helium atoms constant, H:He=220:18. We deliberately used a small number of heavy element atoms – from 2 to 12 – in order to stay in the diluted limit where the interaction effects between the heavy species are small. Results for the ternary H-He-Z mixture were systematically compared with the binary H-He mixture from Militzer (2013).

In Fig. 3, we plotted the volume-pressure relationship for different H-He-O mixtures at 10000 K. For a given pressure, adding oxygen to the mixture results in an increase in the total volume. This effect is magnified in Fig. 4 where we plotted the volume difference between the ternary and the binary mixtures as a function of the number of inserted oxygen atoms. For these conditions, the volume difference is an almost perfectly linear function of the number of oxygen atoms. This means that we can define an effective volume per oxygen atom in the H-He mixture, at given pressure P and temperature T , by:

$$v_{\text{O,eff}} = \frac{1}{N_{\text{O}}} [V(N_{\text{H}}, N_{\text{He}}, N_{\text{O}}) - V(N_{\text{H}}, N_{\text{He}})], \quad (2)$$

where V is the volume associated to a mixture of N_{H} hydrogen, N_{He} helium and N_{O} oxygen atoms. Reciprocally, we can determine the volume for arbitrary but small concentration in oxygen by using an isothermal-isobaric additive mixing rule and the aforementioned effective volume of oxygen.

For pressures above 100 GPa and temperatures higher than 5000 K, we observed a linear behavior of the volume

Table 1. Fit parameters of the effective volume as defined in eq. (3). The units of the parameters were chosen so that the temperature is in K, the pressure in GPa and the volume in \AA^3 per species.

Species	a ($\times 10^{-3}$)	b ($\times 10$)	α ($\times 10^{-6}$)	β ($\times 10^{-1}$)
C	1.154	1.899	-4.839	-2.890
N	1.000	2.093	-3.459	-2.990
O	1.040	2.247	-4.119	-2.916
Si	2.901	3.219	-6.792	-2.915
Fe	1.911	1.407	-8.600	-1.754
MgO	4.277	6.302	-5.432	-3.185
SiO ₂	4.180	8.119	-4.411	-2.971

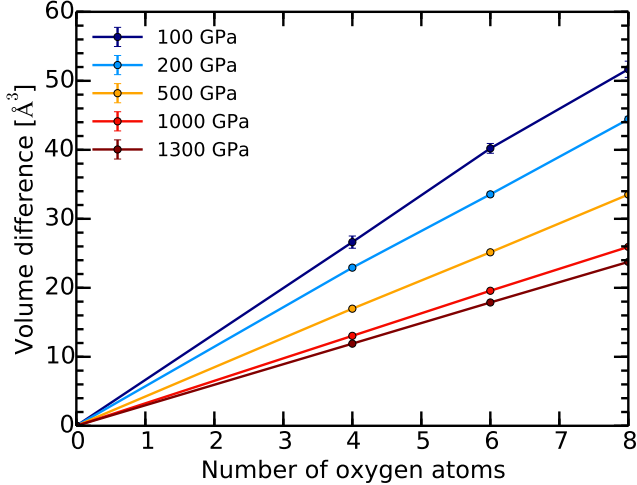


Figure 4. Volume difference between H-He-O and H-He mixtures as a function of the number of oxygen atoms for different pressures ranging from 100 to 1300 GPa and for a temperature of 10000 K.

difference for each species we considered. In Fig. 5 we plotted the effective volume of each species that can be very well fitted as a function of both the temperature and the pressure with the following simple expression:

$$v_{\text{eff}}(P, T) = (aT + b) P^{\alpha T + \beta}, \quad (3)$$

where a , b , α and β are fit parameters given in Tab. (1). To perform this fit we relied on results ranging from 100 to 1500 GPa, from 5000 to 15000 K and for concentrations in heavy elements lower than 5% in number. We first fitted the effective volume as a power-law of the pressure, along different isotherms, and using a weighted least-square fitting procedure. We then fitted the two coefficients of the power-law as an affine function of the temperature – of the form $aT + b$. This provided a robust fit of the effective volume. This fit is an important result of this article because it describes the properties of heavy species under pressure-temperature conditions where H-He mixtures are metallic, which makes up for the major part of giant planet interiors.

We compared the effective volume with the volume of the pure species as available in the literature. We used data from *ab initio* simulations for carbon (Benedict *et al.* 2014), nitrogen (Driver & Militzer 2016), oxygen (Driver *et al.* 2015), iron and magnesium oxide (Wahl *et al.* 2015). Fig. 5 shows a fairly good agreement between the volume of the pure species and their effective volume in H-He mixtures for pressure higher than about 200 GPa. This is not an obvious result as the interactions are mostly between the heavy species and hydrogen or helium in the ternary systems while they are only between the heavy elements themselves in the pure systems. On the other hand, below 200 GPa, some deviations have to be noted.

We also compared the effective volume of an SiO_2 unit with the sum of the effective volumes of one silicon and two oxygen atoms in H-He mixtures. As shown on Fig. 5, there is a very good agreement between the two estimates, which suggests that, under these conditions, the system is most likely dissociated. We infer that a similar behavior is to be expected to any multi-component system that would dissociates with increasing temperature and pressure.

We explored lower pressure-temperature range as well, from 10 to 150 GPa and 2000 to 5000 K. In some cases for these conditions, the relationship between the volume difference and the number of the entities deviates from a perfect linear relationship. We think that these deviations may come from the finite duration of our simulations which may prevent to reach a perfect chemical equilibrium. We still determined an effective volume per species through a linear fit and the results are presented in Fig. 7. To estimate the uncertainty on the effective volume, we combined the intrinsic statistical uncertainty of the effective volume with an estimate of the misfit. For the latter, we computed the effective volumes, $v_{\text{eff},i} = \Delta V(N_{Z,i})/N_{Z,i}$, from our simulations with different numbers of heavy species, $N_{Z,i}$. We then calculated their standard deviation from the linear fit value to characterize the misfit. While the statistical uncertainty is not very sensitive to the temperature or the pressure, the combined uncertainty of the effective volumes increases if the temperature decreases, which can be seen in Fig. 7.

Unlike for the high temperature and pressure conditions, the effective volume of each species does not evolve monotonically as a function of the pressure in the range of 10 to 150 GPa and 2000 to 5000 K, and an important variability can be observed. It is known that in this regime, hydrogen undergoes a dissociation and a metalization (Caillabet *et al.* 2011; Vorberger *et al.* 2007). By identifying the nearest neighbors over time as in Soubiran & Militzer (2015a), we determined an estimate of the dissociation fraction of hydrogen in the H-He mixtures. In Fig. 7, we see a clear correlation between the drastic changes of the effective volume of the heavy species and the dissociation of hydrogen. This result is not surprising because the interactions between an H_2 molecule and a heavy atom are quite different from the interactions between an hydrogen ion and the same heavy element.

More specifically, the effective volume increases by nearly 25% for C, N, O between 60 to 80 GPa at 3000 K, which could also be linked to chemical reactions with the surrounding hydrogen. At low temperature and pressure, for instance, carbon tends to form CH_x molecules with x ranging from 0 to 4 (Sherman *et al.* 2012) and oxygen associates to hydrogen to form hydroxide or water molecules (Soubiran & Militzer 2015b). This chem-

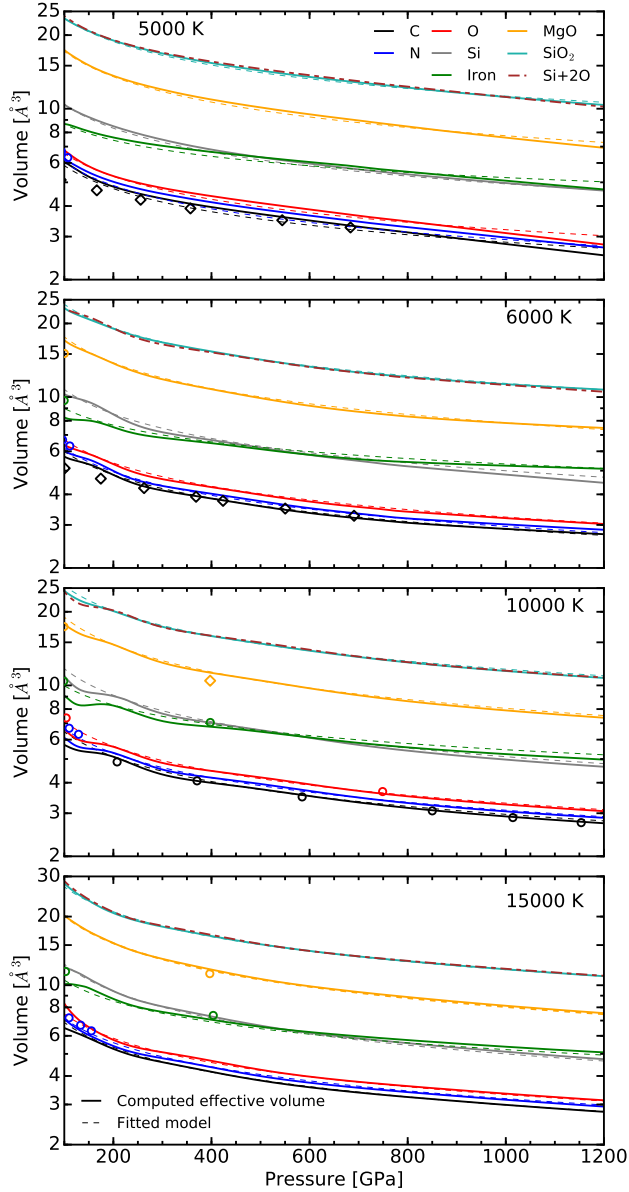


Figure 5. Effective volume for each species in a H-He mixture as a function of the pressure for temperatures from 5000 to 15000 K. The full curves are the direct results from the volume difference analysis. The light green dash-dotted curve is the sum of the volumes of one Si and two O to be compared with the volume of one SiO_2 . The dashed curves represent the fit based on eq. (3) and the parameters given in Tab. (1). The squares (resp. diamonds) represent the volume per species in a pure liquid (resp. solid) phase (Benedict *et al.* 2014; Driver & Militzer 2016; Driver *et al.* 2015; Wahl *et al.* 2015).

istry can also explain the strong deviations of the effective volume of these species from the volume of the pure species. It is also interesting to note that iron has a negative effective volume at the lowest pressure conditions. We attribute this behavior to a complex chemistry with hydrogen. In the case of SiO_2 we also see a variability in the effective volume but more importantly, we see that

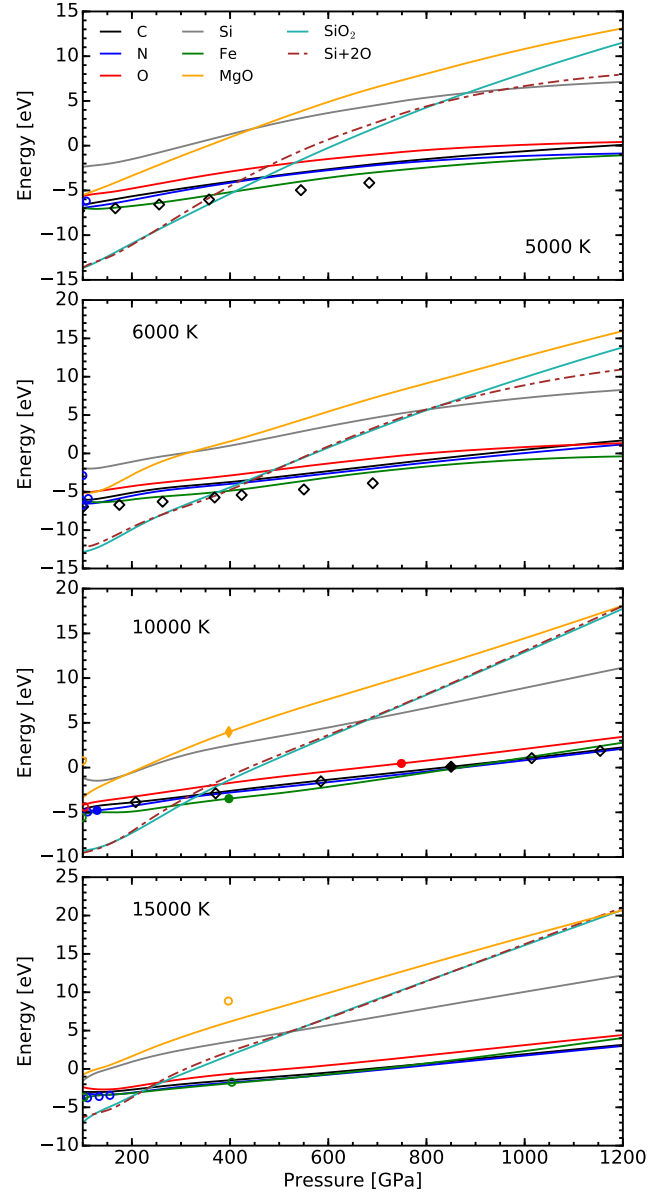


Figure 6. Effective energy for each species in a H-He mixture as a function of the pressure for temperatures from 5000 to 15000 K. The legend is similar to Fig. 5. At 10000 K, the colored symbols represent the data for which we forced the energy to match our data to compensate for any difference in the energy reference.

there are some deviations from the sum of the effective volumes of one Si and two O atoms. This means that the system is not dissociated which modifies the interactions with the H-He mixtures.

The high variability of the effective volume makes it impossible to give a simple fitting formula but we make our results on the effective properties available in the supplementary material attached to this article. Nevertheless, Fig. 7 shows that the formula from eq. (3) with the parameters from Tab. 1, fitted on the results above 5000 K and 100 GPa, actually well reproduces the lower-

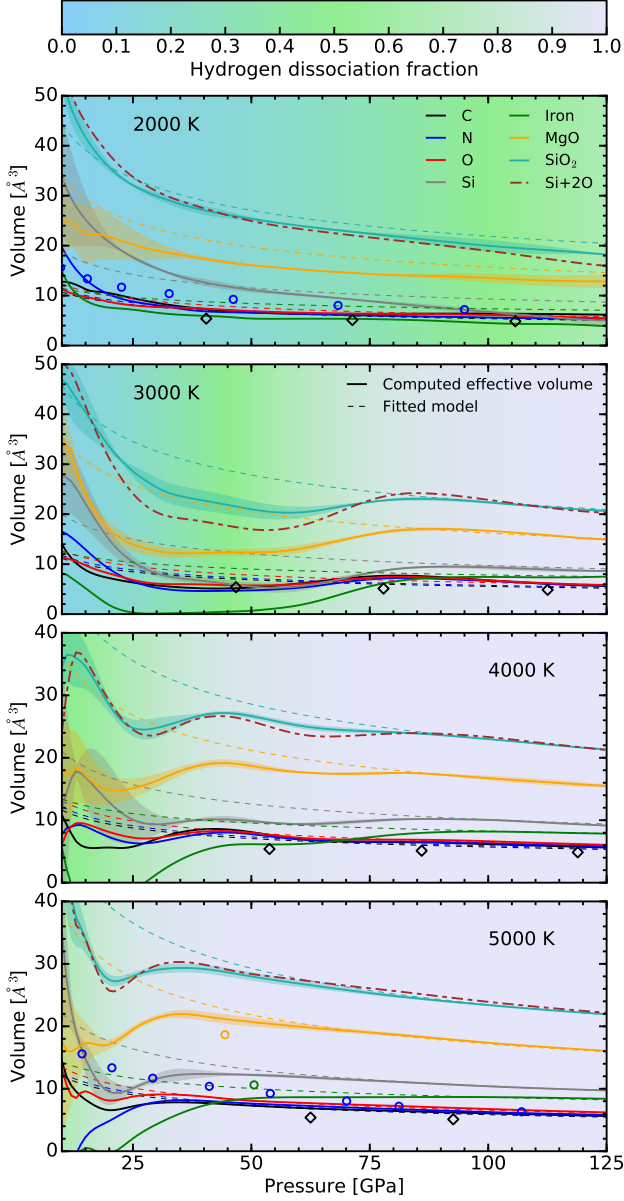


Figure 7. Effective volume for each species in a H-He mixture as a function of the pressure for temperatures from 2000 to 5000 K. The legend is similar to Fig. 5. The colored background represents the dissociation fraction of hydrogen in the H-He mixture (See Fig. 9 for the actual location of the dissociation in Jupiter). The shaded regions around the Si, MgO and SiO₂ curves show the estimated uncertainty.

temperature behavior in the dissociated phase. Namely, at 5000 K, the fit gives reasonable values starting at 50 GPa, and at 4000 and 3000 K, it gives accurate results from 80 to 150 GPa.

3.2. Effective internal energy

We investigated the effect of the inclusion of heavy elements in H-He mixtures on the internal energy of the systems. Since the energy is an extensive thermodynamic function like the volume, we followed the same procedure as in the previous section. The energy differ-

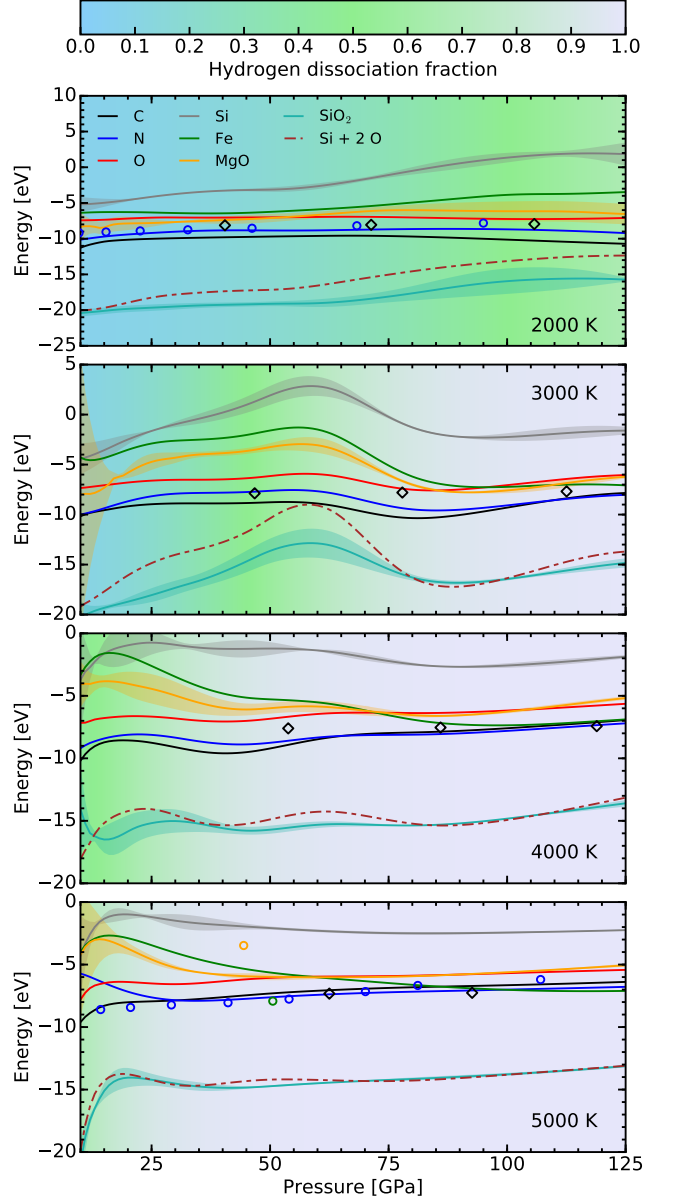


Figure 8. Effective energy for each species in a H-He mixture as a function of the pressure for temperatures from 2000 to 5000 K. The legend is similar to Fig. 7.

ence between the ternary and the binary mixtures exhibits a fairly linear behavior as a function of the number of heavy element entities (graph not shown). By comparing the energy of the ternary mixture of N_H hydrogen atoms, N_{He} helium atoms and N_Z Z entities (atoms or molecules) with the energy of the binary H-He mixture at the same pressure P and temperature T , we were able to determine an effective energy per species Z:

$$e_{z,\text{eff}} = \frac{1}{N_Z} [E(N_H, N_{He}, N_Z) - E(N_H, N_{He})]. \quad (4)$$

Our results for the effective energies are plotted in Fig. 6 and 8. In the dissociated regime, the effective energy exhibits a fairly smooth evolution with low devi-

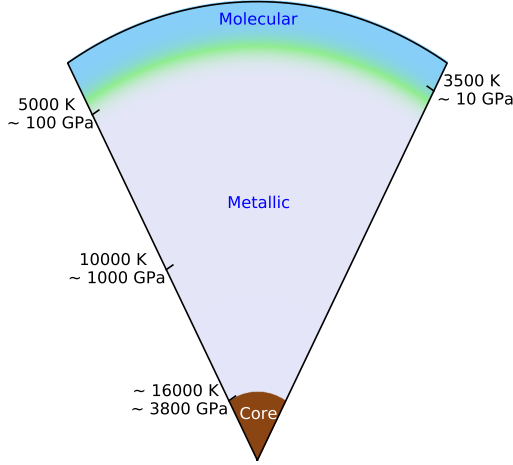


Figure 9. Schematic view of the interior of Jupiter with the colors indicating the dissociation of hydrogen as in Figs. 7 and 8. We also indicated the order of magnitude of the thermodynamic conditions at different depths.

ations from the linear behavior. We compared the effective energy with the internal energy of the pure species. In order to correct for any shift in the origin of the energy between the different data sources, we artificially made them to coincide at 10000 K, temperature at which we had the most data and where we expect every species to be dissociated. The full symbols in Fig. 6 indicate the specific data we forced to match the effective energies we computed. This results in an artificially good match on the 10000 K isotherm. However, if we look at the other temperatures, we observe some strong deviations between the effective energy and the pure species energy, emphasizing the importance of the inter-species interactions. Below 5000 K, the effective energy exhibits similar features to the effective volume with drastic variations as a function of the pressure when hydrogen undergoes its dissociation.

Overall, we observe that the energy of the ternary mixtures can be approximated by an isothermal-isobaric additive mixing rule which is very helpful for evolution models of planets. However, the effect of the dilution of the heavy species into the H-He cannot be neglected, since the effective energy is substantially different from the internal energy of the pure species.

3.3. Effective entropy

In order to determine the influence of the heavy elements on the temperature-pressure profile of the giant planets, one needs to compute the entropy of the ternary mixtures. Hence, we computed the entropy of ternary mixtures using thermodynamic integrations. As the computation cost of such calculations is very high, we only performed it for oxygen in H-He mixtures and for a subset of temperatures. We shall see in Section 4

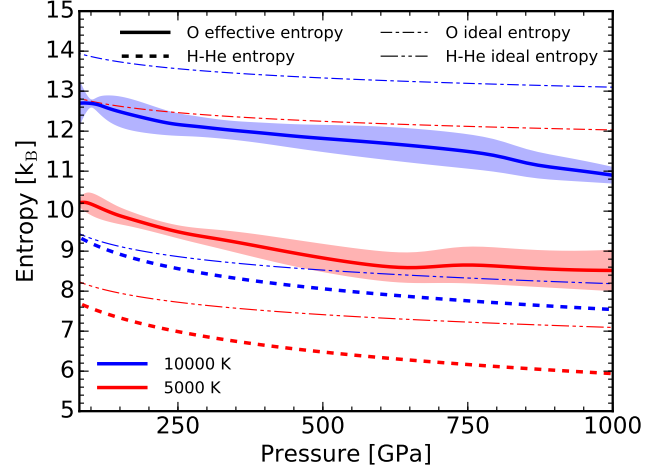


Figure 10. Effective entropy per oxygen atom in a ternary H-He-O mixtures as a function of the pressure, for 5000 and 10000 K. The shaded region represents our estimate of the uncertainty. We also plotted in dashed lines the entropy per nucleus for the binary H-He mixture under the same conditions. For comparison, the thin lines show the ideal entropy of pure oxygen and of the H-He mixture under equivalent density and temperature conditions.

that it is already enough to determine the effect on the density profile.

We followed the same procedure as for the volume and the energy: we computed the entropy of the mixture for different concentrations and compared the results with the binary H-He mixture. However, the entropy encompasses not only the entropy of each species but also a mixing entropy. We therefore defined the effective entropy based on the total entropy of the ternary mixtures of N_H hydrogen atoms, N_{He} helium atoms and N_O oxygen atoms and the entropy of the H-He binary mixture, at constant pressure P and temperature T , by:

$$s_{O,eff} = \frac{1}{N_O} [S(N_H, N_{He}, N_O) - S(N_H, N_{He}) - \Delta S_{mix}(N_H, N_{He}, N_O)], \quad (5)$$

where the entropy of mixing is given by:

$$\begin{aligned} \Delta S_{mix}(N_H, N_{He}, N_O) &= k_B \ln(N_H + N_{He} + N_O)! \\ &\quad - k_B \ln(N_H + N_{He})! \\ &\quad - k_B \ln N_O!. \end{aligned} \quad (6)$$

We chose this formula with the explicit factorial term because the usual Sterling approximation is not appropriate for small numbers.

We plotted the effective entropy of oxygen in Fig. 10. The uncertainty is slightly higher than on the energy or the volume because the entropy calculation requires more computation steps but it remains very reasonable overall, as the maximum uncertainty does not exceed 6 %. We also plotted the entropy per nucleus of the binary H-He mixtures under the same conditions. For

comparison we computed the ideal entropy of the H-He mixture and of oxygen using the Sackur-Tetrode formula (Reichl 1998):

$$S_{\text{id}} = k_B \sum_{\alpha} x_{\alpha} \left(\ln \left[v_{\alpha} \left(\frac{m_{\alpha} k_B T}{2\pi \hbar^2} \right)^{3/2} \right] + \frac{5}{2} \right), \quad (7)$$

where x_{α} , v_{α} and m_{α} are the concentration ratio, volume per particle and mass per particle of the particles of type α respectively. We used the P - V relationship of the H-He mixture to derive the ideal entropy of H-He as a function of the pressure. For oxygen, we based our calculation on the effective volume as derived in section 3.1.

The effective entropy of oxygen is higher than the entropy of H-He, which is simply a mass effect, which is present in the ideal entropy. Both the effective entropy of oxygen and entropy of H-He are smoothly decreasing as pressure increases because the volume per nucleus decreases. The non-ideal effects – the difference between actual and ideal entropy – increase with pressure because the interactions introduce some local order. The entropy and effective entropy increase as temperature increases consistently with the ideal entropy although the increase is lower for the ideal entropy. We also note that as the temperature increases, the non-ideal effects decreases, which is consistent with a diminution of the interactions effects. We observe that the non-ideal effects appear more pronounced on the oxygen than on the H-He mixture. But we have to stress that this is here only an effective entropy of a single oxygen atom in a H-He fluid and that the entropy of pure oxygen under similar conditions may be quite different. The interactions with hydrogen and helium may also influence the local ordering around the oxygen atoms modifying the entropy. Last, we want to stress that the variations in entropy or effective entropy as a function of the pressure and the temperature are quite similar for H-He and for oxygen, which is important when determining the internal profile of a giant planet.

4. DISCUSSION

The analysis of the *ab initio* simulations of several ternary mixtures showed that, in the diluted regime, the addition of heavy elements to an H-He mixtures can be very well described by an ideal isothermal-isobaric additive mixing rule as long as we employ the effective properties of the heavy materials as presented in the previous section. For the higher pressures in the dissociated regime, the effective volume coincides with the volume of the pure systems but deviations are observed for lower pressures emphasizing the need for these effective properties.

In the diluted limit, we can also expect that we can approximate the properties of a multi-component sys-

tem by simply adding the effective volumes or energies of each component separately, because the cross-interactions between different heavy elements should be negligible compared to the interactions with hydrogen and helium. This is further supported by the good agreement between the SiO_2 effective properties and those of silicon and oxygen taken separately. This approximation is however only accurate for the dissociated regime, which actually represent a significant mass fraction of the interiors of Jupiter and Saturn. All the previous calculations were performed for a fixed hydrogen to helium ratio, but the deviations from the pure species properties are small enough to let us believe that the deviations on the effective properties, induced by a reasonable change in helium concentration, should be mostly negligible.

Using the results of our calculations, we studied the consequences of adding heavy elements in the hydrogen and helium rich envelope of giant planets. As a toy model, we considered as a starting point an homogeneous fully convective H-He envelope with a composition of H:He=220:18 as employed in our simulations. We picked the temperature at 1 bar to be $T = 165$ K, which is close to the Jupiter measured value of 166.1 K (Seiff *et al.* 1998), for instance. With this condition and using Militzer (2013) and Saumon *et al.* (1995) EOSs, we were able to determine the pressure-temperature profile, plotted in Fig. 12. We also computed the density along the isentrope $\rho_{\text{H-He}}(P)$.

With the effective volumes in Tab. (1), we computed the excess density induced by the addition of a $Z = 0.02$ mass fraction of different heavy elements homogeneously throughout the H-He envelope. The pressure-temperature profile was kept constant as in Hubbard & Militzer (2016), and we only perturbed the density.

In Fig. 11, we displayed the relative density difference between the enriched envelope and the original H-He envelope $[\rho_{\text{H-He-Z}}(P) - \rho_{\text{H-He}}(P)]/\rho_{\text{H-He}}(P)$. The curves are all for the same mass fraction, $Z = 0.02$, but for different materials. They illustrate by how much the multi-component mixture deviates from the H-He mixture. In the most extreme case, when heavy atoms have a negligible volume, a 2% mass fraction leads to a 2% density change. As expected, the densest species – iron and silicon dioxide – introduce the largest density change, close to a 2% density increase for a 2% mass fraction. On the other hand, the inclusion of Synthetic Uranus (SU) induces a 1% density increase only. SU is a proxy that we used to mimic a mixture of ice derivatives based on oxygen, nitrogen, carbon and hydrogen in a ratio of H:O:C:N=87:25:13:4. It was first introduced as a proxy for Uranus interior in high pressure laboratory experiments (Nellis *et al.* 1997), and it was also used in the recent Jupiter model by Hubbard & Militzer (2016) to enrich the envelope. The relatively low density of SU

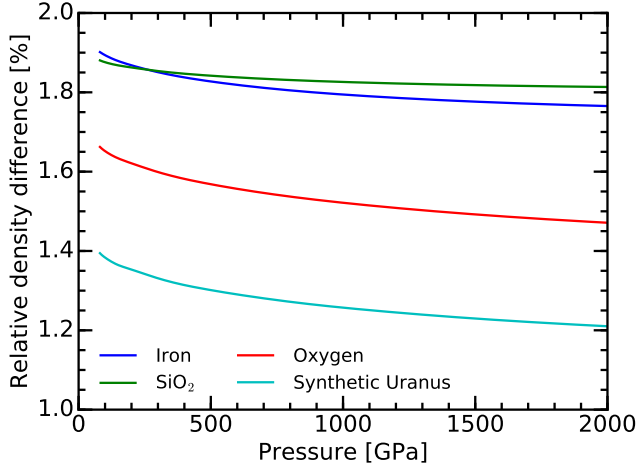


Figure 11. Relative density difference, along the H-He isentrope of a giant planet with $T = 165$ K at 1 bar, between a simple H-He mixture and a multi-component mixture including a 2 % mass fraction of heavy elements. Synthetic Uranus refers to a mixture of ice derivatives as presented in [Nellis *et al.* \(1997\)](#); [Hubbard & Militzer \(2016\)](#). For this species, we chose a composition of H:O:C:N=87:25:13:4.

is due to the presence of a high amount of hydrogen that we chose to include in the computation of the Z fraction. For comparison, oxygen has a slightly higher density with a density increase of roughly 1.5%.

We showed that the addition of heavy elements in the H-He mixture slightly influenced the density of the mixture. It is thus natural to infer that they may have an influence on the entropy as well, and thus, on the pressure-temperature profile of the envelope. Yet, a change in the P - T relationship in the planet would also change its density profile and it has to be accounted for. Besides the case of the unperturbed H-He isentrope in Fig. 12, we explored three different scenarios for the enriched layer. The first scenario is a single layer of a H-He-O mixture with a $Z = 0.02$ mass fraction in oxygen but this time taking the entropy change into account. We then explored two other scenarios with a two-layer picture where the outer layer is made of H-He solely and the inner layer is an enriched H-He mixture with 2% of oxygen. The difference lies in the temperature at the interface between the two layers: in one case we considered a 3500 K interface, in the other we picked 5000 K. The resulting properties for the different scenarios are summarized in Tab. (2).

For the first scenario, we assumed that the oxygen reacted with the surrounding hydrogen at 165 K and 1 bar to form water molecules. We further assumed that water is in a vapor state as the concentration is low. We then could compute the entropy of the mixture at 165 K and 1 bar by:

$$s = x_{\text{H}_2} s_{\text{H}_2} + x_{\text{He}} s_{\text{He}} + x_{\text{H}_2\text{O}} s_{\text{H}_2\text{O}} - k_B (x_{\text{H}_2} \ln x_{\text{H}_2} + x_{\text{He}} \ln x_{\text{He}} + x_{\text{H}_2\text{O}} \ln x_{\text{H}_2\text{O}}), \quad (8)$$

where x_α (resp. s_α) is the number fraction (resp. entropy per molecule) of molecules of type α . We used [Saumon *et al.* \(1995\)](#) EOS to compute the entropy of H and He. For water, we used the entropy from the translational, rotational and vibrational degrees of freedom as in [Vidler & Tennyson \(2000\)](#). We obtained an entropy of 7.607 k_B /nucleus for the whole mixture.

Following a constant entropy line, and using the effective entropy of oxygen computed in Section 3.3, we were able to compute the P - T relationship above 4000 K and 10 GPa, as represented in Fig. 12. The comparison with the unperturbed isentrope shows that the oxygen entropic effects result in an increase of the pressure by 3% for a given temperature. Equivalently, it results in a temperature decrease of roughly 80 K at constant pressure. The effect on the density can be seen in Fig. 13: compared to the original H-He profile, the density variation induced by the oxygen increases from 1.5% without the entropy correction to 1.6% when taking the entropy of oxygen into account. Since this is a rather marginal effect, it is hard to believe that this difference could be resolved by Juno measurements of the gravitational moments. We find it reasonable to use the original H-He isentrope for giant planet modeling ([Hubbard & Militzer 2016](#)).

The second and third scenarios are based on a two-layer picture with a pure H-He outer envelope and an inner envelope with a 2% mass fraction of oxygen. The outer layer has the unperturbed P - T profile and the enriched inner layer profile is determined by the condition at the interface: we computed the entropy of the ternary H-He-O mixture assuming that, at the interface, the pressure and the temperature were the same in both layers. The resulting profiles are represented by the symbols in Figs. 12 and 13. If we let the inner layer start in the molecular phase, at 3500 K and 7.2 GPa, we retrieve to a very good accuracy the predictions of the single layer. It is mostly the dissociation that drives the slight shift in the isentrope and it occurs at temperatures higher than 3500 K. On the other hand, if we

Table 2. Properties of the hypothetical isentropes in an H-He envelope enriched with 2% oxygen in mass and with a 165 K temperature at 1 bar. The first two models are for a single layer without or with entropy correction. The last two models are for a two-layer picture with the enriched layer only for temperatures higher than 3500 or 5000 K. For each hypothesis, we give the entropy per nucleus S as well as the pressures at 5000 and 10000 K.

Description	S (k_B /nucl.)	$P_{5000\text{K}}$ (GPa)	$P_{10000\text{K}}$ (GPa)
Unperturbed H-He	7.598	95.6	927
H-He-O mono-layer	7.607	98.6	950
H-He-O starts at 3500 K	7.605	98.9	953
H-He-O starts at 5000 K	7.624	95.6	929

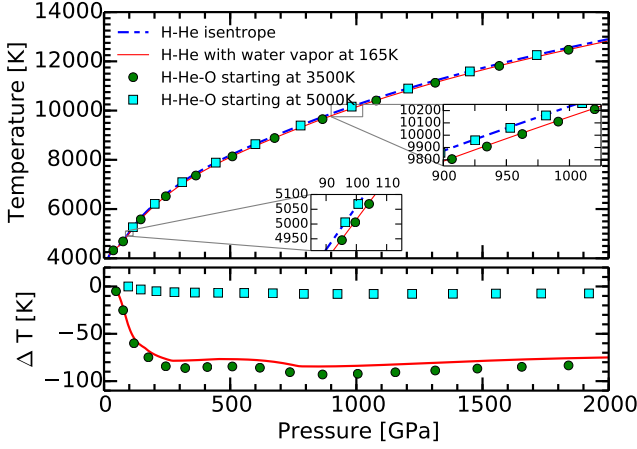


Figure 12. Pressure-temperature profile in the H-He envelope of a gaseous planet with $T = 165$ K at 1 bar with a 2% mass fraction of oxygen. The full and dashed lines are for a single layer of H-He-O with or without entropy correction due to the presence of oxygen. The discrete symbols are for a two-layer picture, where the 2% oxygen enriched layer starts at 3500 or 5000 K. A summary of the properties of these profiles can be found in Tab. (2). The bottom graph shows the temperature difference between the different profiles with the original H-He profile.

let the inner layer start at 5000 K and 95.6 GPa, in the dissociated phase, the predicted isentrope is almost exactly the same as the H-He isentrope. The temperature difference is lower than 10 K at a given pressure and the pressure is increased by only 0.2% at 10000 K (see Tab. (2)). The entropy itself is modified by the presence of oxygen, but this shift is nearly constant along the H-He isentrope in the dissociated phase, which explains the absence of impact on the predicted pressure-temperature profile and thus on the density. We expect this observation to be true for the other heavy element as well, especially in the diluted limit.

The last scenario with the temperature at the interface at 5000 K is of interest for cold giant planet modeling. When the planet is cold enough, a phase separation of hydrogen and helium is indeed expected to occur, naturally differentiating the envelope in (at least) two layers. The innermost layer and helium enriched is entirely in the dissociated regime (Guillot 2005; Hubbard & Militzer 2016) and is also the one the most subject to heavy element enrichment because in direct contact with the eroding core. Yet, we showed on the example of oxygen that in this regime, the entropy of the heavy element play virtually no role on the pressure-temperature profile that can thus be determined by the H-He properties solely. This means that to model this innermost layer, the H-He EOS and the effective volumes of the heavy elements are sufficient to properly recover the density profile.

5. MASS-RADIUS RELATIONSHIP

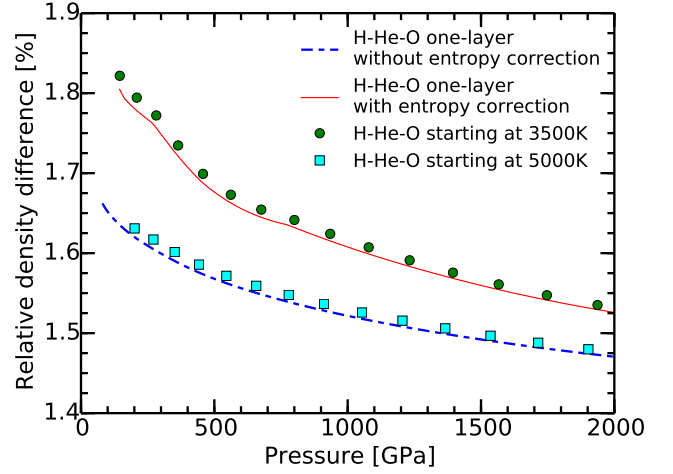


Figure 13. Relative density difference between a simple H-He mixture and a multi-component mixture including a 2% mass fraction of oxygen along the P - T profile of the envelope of a giant planet with a 165 K temperature at 1 bar. The dashed blue (resp. solid red) curve shows the density increase for a single layer without (resp. with) the entropy correction due to the oxygen. The green circles (resp. cyan squares) are for a two-layer hypothesis with an outer H-He layer and an inner H-He-O layer starting at 3500 K (resp. 5000 K). The corresponding P - T profiles are those of Fig. 12.

In this section, we briefly discuss the effects that heavy elements have on the mass-radius relationship of gas giant exoplanets. To simplify our analysis, we only consider planets without a rocky core and assume a homogeneous, convective interior. The adiabatic P - T profile is derived from a H-He mixture starting from 1 bar and 166.1 K. For a given planet mass, the radius is derived by solving the ordinary differential equations of the hydrostatic equilibrium (Seager *et al.* 2007; Wilson & Militzer 2014). Fig. 14 shows the effect that the introduction of a 2% and a 4% mass fraction of oxygen has on the radius of a giant planet. We find that a Jupiter-mass planet respectively shrinks by 0.7% and 2.4% in radius. According to eq. (3), the introduction of oxygen not only increases the mass but also the volume of the H-He mixture at given pressure and temperature. As a result, the density increases by less than 2% or 4%; respectively. In order to disentangle both effects, we plot the mass-radius relationship for planets where we have increased the H-He density by 2% and 4% in Fig. 14. We find that a Jupiter-mass planet then shrinks by 1.7% and 3.3% in radius; respectively.

It is interesting to note that the effect of heavy elements is much larger if one compares different planet masses for a given radius. Since giant planets have degenerate interiors, their radii start to shrink if a mass of approximately 3 Jupiter masses is exceeded. Jupiter's radius is not too different from the maximum radius of approximately $1.2 R_J$ (Seager *et al.* 2007). The slope of the mass-radius curves in Fig. 14 is thus relatively small

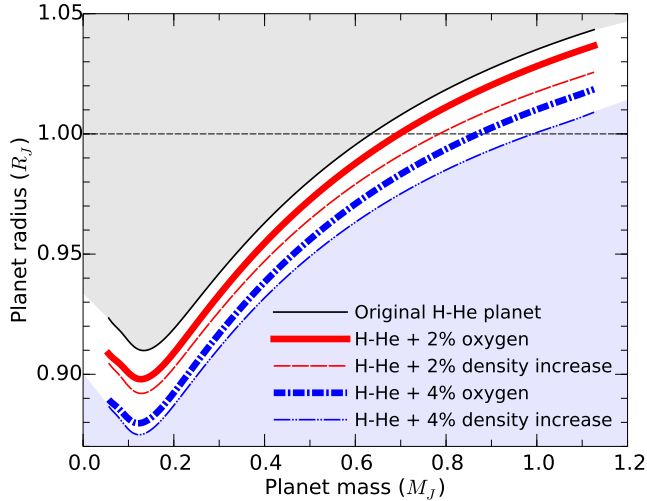


Figure 14. Mass-radius relationship in Jupiter units for giant planets without a rocky core. The adiabatic interior P - ρ - T profiles are derived from H-He mixture with an effective temperature of 166.1 K at 1 bar. The thin solid line shows the radii of the H-He planets without heavy elements. The thin dashed lines illustrate the effect that a 2% or 4% increase in density has on the planet radius. The thick lines show the effect of introducing a 2% and 4% mass fraction of oxygen.

and a modest change in radius has a significant effect on the inferred planet mass. For a fixed radius of $1 R_J$, the mass of a core-less planet increases from 0.63 to 0.70 or 0.86 M_J if an oxygen mass fraction of 2% or 4% is introduced; respectively.

6. CONCLUSIONS

Ab initio simulations showed that, in the diluted limit, ternary mixtures made of hydrogen and helium in roughly solar abundance with heavy elements can be very well approximated by an isothermal-isobaric additive mixing rule on the volume and the energy under thermodynamic conditions relevant in the interior of giant planets. It is however necessary to use effective

volume and energy for the heavy elements because the dominant contributions come from the cross-interactions with hydrogen and helium. Although these effective properties tend towards the pure species volume and energy at high pressure and temperature, there are significant discrepancies at lower pressure and temperature.

The study of the entropy of oxygen showed that in the diluted limit, the effective entropy is mostly influenced by the dissociation of hydrogen but stays rather constant along the H-He isentrope in the dissociated regime. If we consider a H-He giant planet with a 2% oxygen mass fraction, the net increase in density is of about 1.5% compared to a pure H-He envelope, for given pressure and temperature. Including the entropy correction, the addition of 2% oxygen increases the pressure by roughly 3% at a given temperature or, equivalently, decreases the temperature by less than 2% at a given pressure. The effect of the entropy is thus very small and the net over-density is only of the order of 0.1%.

In the case of a two-layer model with an upper layer made of H-He and an oxygen enriched inner layer entirely in the metallic regime, the predicted pressure-temperature profile do not deviate from the pure H-He predictions. Overall, in the diluted limit, the entropy appears to have very little effect on the density-pressure relationship.

We argue that the use of the isentrope properties of the H-He mixture with the effective volume and energy of the heavy elements as described in this article should give a very good approximation of the actual profile of giant planets. The comparison with the coming data on the gravitational moments should help to constrain the distribution of heavy elements in these planets.

ACKNOWLEDGMENTS

This work was supported by NASA and NSF. Computers at NAS, XSEDE and NCCS were used.

REFERENCES

- Baldereschi, A. 1973, PhRvB, 7, 5212.
 Baraffe, I., Chabrier, G. & Barman, T. 2008, A&A 482, 315.
 Baraffe, I., Chabrier, G. & Barman, T. 2010, RPPH 73, 016901.
 Benedict, L. X., Driver, K. P., Hamel, S., Militzer, B., Qi, T., Correa A. A., Saul, A. & Schwegler, E. 2014, PhRvB, 89, 224109.
 Blöchl, P. E. 1994, PhRvB, 50, 17953.
 Bolton, S. J. 2010. The Juno Mission. Proceedings of the International Astronomical Union, 6, pp 92-100.
 Brygoo, S., Millot, M., Loubeyre, P., Lazicki, A. E., Hamel, S., Qi, T., Celleirs, P. M., Coppari, F., Eggert, J. H., Fratanduono, D. E., Hicks, D. G., Rygg, J. R., Smith, R. F., Swift, D. C., Collins, G. W. & Jeanloz, R. 2015, JAP, 118, 195901.
 Caillabet, L., Mazevet, S. & Loubeyre, P. 2011, PhRvB, 83, 094101.
 Denœud, A., Benuzzi-Mounaix, A., Ravasio, A., Dorchie, F., Leguay, P. M., Gaudin, J., Guyot, F., Brambrink, E., Koenig, M., Le Pape, S. & Mazevet, S. 2014, PhRvL, 113, 116404.
 Driver, K. P., Soubiran, F., Zhang, S. & Militzer, B. 2015, JChPh, 143, 164507.
 Driver, K. P. & Militzer, B. 2016, PhRvB, 93, 064101.
 Fortney, J. J. & Hubbard, W. B. 2004, ApJ, 608, 1039.
 Fortney, J. J., Mordasini, C., Nettelmann, N., Kempton, E. M.-R., Greene, T. P. & Zahnle, K. 2013, ApJ, 775, 80.
 Fuller, J., Lai, D. & Storch, N. I. 2014, Icar, 231, 34.
 Fuller, J. 2014, Icar, 242, 283.
 Gaulme, P., Schmider, F.-X., Gay, J., Guillot, T. & Jacob, C. 2011, A&A, 531, A104.

- González-Cataldo, F., Wilson, H. F. & Militzer, B. 2014, *ApJ*, 787, 79.
- Guillot, T. 2005, *AREPS*, 33, 493.
- Guillot, T. & Gautier, D. 2015. Giant Planets. In: Schubert, G. (Ed.), *Treatise on Geophysics* (2nd Edition). Elsevier, Oxford, pp. 529 - 557.
- Helled, R. & Guillot, T. 2013, *ApJ*, 767, 113.
- Hohenberg, P. & Kohn, W. 1964, *PhRv*, 136, 864.
- Hubbard, W. B. & Militzer, B. 2016, *ApJ*, 820, 13.
- Jones, D. L., Folkner, W. M., Jacobson, R. A., Jacobs, C. S., Dhawan, V., Romney, J. & Fomalont, E. 2015, *AJ*, 149, 28.
- Kohn, W. & Sham, L. J. 1965, *PhRv*, 140, 1133.
- Kresse, G. & Furthmüller, J. 1996, *PhRvB*, 54, 11169.
- Leconte, J. & Chabrier, G. 2012, *A&A* 540, A20.
- Leconte, J. & Chabrier, G. 2013, *NatGe* 6, 347.
- Lodders, K. 2003, *ApJ*, 591, 1220.
- Lorenzen, W., Holst, B. & Redmer, R. 2009, *PhRvL*, 102, 115701.
- Lorenzen, W., Holst, B. & Redmer, R. 2011, *PhRvB*, 84, 235109.
- McMahon, J. M., Morales, M. A., Pierleoni, C. & Ceperley, D. M. 2012, *RvMP*, 84, 1607.
- Mermin, N. D. 1965, *PhRv*, 137, A1441.
- Militzer, B. 2009, *PhRvB*, 79, 155105.
- Militzer, B. 2013, *PhRvB*, 87, 014202.
- Militzer, B. & Hubbard, W. B. 2013, *ApJ*, 774, 148.
- Militzer, B. & Driver, K. P. 2015, *PhRvL*, 115, 176403.
- Morales, M. A., Pierleoni, C., Schwegler, E. & Ceperley, D. M. 2009, *PNAS*, 106, 1324.
- Morales, M. A., Hamel, S., Caspersen, K. & Schwegler, E. 2013, *PhRvB*, 87, 174105.
- Nellis, W., Holmes, N., Mitchell, A., Hamilton, D., & Nicol, M. 1997, *JChPh*, 107, 9096.
- Nettelmann, N., Becker, A., Holst, B. & Redmer, R. 2012, *ApJ*, 750, 52.
- Nettelmann, N., Helled, R., Fortney, J. & Redmer, R. 2013, *P&SS*, 77, 143.
- Nosé, S. 1984, *JChPh*, 81, 511.
- Nosé, S. 1991, *PThPS*, 103, 1.
- Perdew, J. P., Burke, K. & Ernzerhof, M. 1996, *PhRvL*, 77, 3865.
- Pollack, J. B., Hubickyj, O., Bodenheimer, P., Lissauer, J. J., Podolak, M. & Greenzweig, Y. 1996, *Icar*, 142, 62.
- Rapaport, D. C. 2004, *The Art of Molecular Dynamics Simulation*, Cambridge University Press.
- Reichl, L. E. 1998, *A modern course in statistical physics*, 2nd ed., Wiley-Interscience.
- Saumon, D., Chabrier, G. & van Horn, H. M. 1995, *ApJSS*, 99, 713.
- Schneider, J., Dedieu, C., Sidaner (Le), P., Savalle, R. & Zolotukhin, I. 2011, *A&A*, 532, A79.
- Seager, S., Kuchner, M., Hier-Majumder, C. A. & Militzer, B. 2007, *ApJ*, 669, 1279.
- Seiff, A., Kirk, D. B., Knight, T. C. D., Young, R. E., Mihalov, J. D., Young, L. A., Milos, F. S., Schubert, G., Blanchard, R. C. & Atkinson 1998, *JGR*, 103, 22857.
- Sherman, B. L., Wilson, H. F., Weerartane, D. & Militzer, B. 2012, *PhRvB*, 86, 224113.
- Soubiran, F., Mazevet, S., Winisdoerffer, C. & Chabrier, G. 2013, *PhRvB*, 87, 165114.
- Soubiran, F. & Militzer, B. 2015, *ApJ*, 806, 228.
- Soubiran, F. & Militzer, B. 2015, *HEDP*, 17, 157.
- Stevenson, D. J. & Salpeter, E. E. 1977, *ApJS*, 35, 239.
- Stevenson, D. J. 1982, *P&SS*, 30, 775.
- Vidler, M. & Tennyson, J. 2000, *JChPh*, 113, 21.
- Vorberger, J., Tamblyn, I., Militzer, B. & Bonev, S. A. 2007, *PhRvB*, 75, 024206.
- Wahl, S. M., Wilson, H. F. & Militzer, B. 2013, *ApJ*, 773, 95.
- Wahl, S. M., Wilson, H. F. & Militzer, B. 2015, *E&PSL*, 410, 25.
- de Wijs, G. A., Kresse, G. & Gillan, M. J. 1998, *PhRvB*, 57, 8223.
- Wilson, H. F. & Militzer, B. 2010, *PhRvL*, 104, 121101.
- Wilson, H. F. & Militzer, B. 2012, *ApJ*, 745, 54.
- Wilson, H. F. & Militzer, B. 2012, *PhRvL*, 108, 111101.
- Wilson, H. F. & Militzer, B. 2014, *ApJ*, 973, 34.
- Wong, M. H., Mahaffy, P. R., Atreya, S. K., Niemann, H. B. & Owen, T. C. 2004, *Icar*, 171, 153.
- Wright, J. T., Fakhouri, O., Marcy, G. W., Han, E., Feng, Y., Johnson, J. A., Howard, A. W., Fischer, D. A., Valenti, J. A., Anderson, J. & Piskunov, N. 2011, *PASP*, 123, 412.

Table 3. Pressure and internal energy of H-He- Z mixtures with 220 H, 18 He and N_Z heavy entities.

Species	Temperature (K)	N_Z	Volume ($\text{\AA}^3/\text{nucl.}$)	Pressure (GPa)	Internal Energy (eV/nucl.)
C	2000	4	3.88922	42.131 \pm 0.040	-2.48961 \pm 0.00099
C	2000	4	3.21772	65.040 \pm 0.136	-2.30810 \pm 0.00149
C	2000	4	2.72109	95.333 \pm 0.153	-2.09755 \pm 0.00139
C	2000	4	2.36276	127.530 \pm 0.345	-1.84461 \pm 0.00370
C	2000	6	6.23309	14.638 \pm 0.075	-2.81747 \pm 0.00184
C	2000	6	4.74436	27.363 \pm 0.082	-2.68190 \pm 0.00144

NOTE—Table 3 is published in its entirety in the electronic edition of the *Astrophysical Journal*. A portion is shown here for guidance regarding its form and content.

Table 4. Pressure and internal energy of H-He-O mixtures with 220 H, 18 He and N_O O atoms.

Temperature (K)	N_O	Volume ($\text{\AA}^3/\text{nucl.}$)	Pressure (GPa)	Internal Energy (eV/nucl.)	Helmholtz Free Energy (eV/nucl.)
5000	4	2.27838	157.151 \pm 0.133	-1.07385 \pm 0.00128	-4.26949 \pm 0.00067
5000	4	1.67448	317.938 \pm 0.131	-0.43909 \pm 0.00139	-3.42557 \pm 0.00043
5000	4	1.18800	684.367 \pm 0.170	0.73063 \pm 0.00165	-2.00307 \pm 0.00031
5000	6	3.19134	75.024 \pm 0.123	-1.52485 \pm 0.00218	-4.92724 \pm 0.00077
5000	6	2.69878	109.354 \pm 0.115	-1.33611 \pm 0.00202	-4.64932 \pm 0.00075
5000	6	2.25970	164.723 \pm 0.129	-1.07571 \pm 0.00102	-4.28233 \pm 0.00057

NOTE—Table 4 is published in its entirety in the electronic edition of the *Astrophysical Journal*. A portion is shown here for guidance regarding its form and content.

Table 5. Effective properties of heavy elements in H-He mixtures.

Species	Temperature (K)	Pressure (GPa)	Volume (\AA^3)	Internal Energy (eV)	Entropy (k_B)
O	5000	1050	3.018 \pm 0.063	0.196 \pm 0.718	8.51 \pm 0.56
O	5000	1100	2.937 \pm 0.072	0.281 \pm 0.798	8.53 \pm 0.61
O	5000	1150	2.859 \pm 0.081	0.353 \pm 0.879	8.55 \pm 0.68
O	5000	1200	2.784 \pm 0.090	0.413 \pm 0.962	8.57 \pm 0.75
O	6000	100	6.377 \pm 0.082	5.136 \pm 0.210	
O	6000	150	5.853 \pm 0.061	4.740 \pm 0.237	

NOTE—The effective entropy is only available for oxygen and only at 5000 and 10000 K. Table 5 is published in its entirety in the electronic edition of the *Astrophysical Journal*. A portion is shown here for guidance regarding its form and content.